J. Mod. Power Syst. Clean Energy (2015) 3(1):82–92
DOI 10.1007/s40565-014-0093-8

A preliminary study of impact of reduced system inertia in a low-carbon power system

Di WU (✉), Milad JAVADI, John Ning JIANG

Abstract One of the important features of low-carbon electric power system is the massive deployment of renewable energy resources in the advent of a new carbon-strained economy. Wind generation is a major technology of generating electric power with zero carbon dioxide emission. In a power system with the high penetration of wind generation, the displacement of conventional synchronous generators with variable speed wind turbines reduces system inertia. This leads to larger system frequency deviation following a loss of large generation. In this paper, the impact of the reduction of system inertia on system frequency is analyzed as the result of the integration of a significant amount of wind generation into power systems. Furthermore, we present a preliminary study of the impact of the distribution of the inertia contributions from those online conventional synchronous generators on the rate of change of frequency (ROCOF) based on the total energy injected into the system due to the fault. The total fault energy is represented using Hamiltonian formulism. With the IEEE 39-bus system, it is shown that for a fault with the given injected total energy, clearing time, and location, the distribution of inertia contributions can significantly affect the magnitude of ROCOF. Moreover, for such a fault with different locations, the average of the magnitudes of ROCOF caused by the fault at different locations is larger when the distribution of the inertia contributions is more dispersed.

CrossCheck date: 8 December 2014

Received: 3 October 2014 / Accepted: 8 December 2014 / Published online: 31 January 2015

D. WU, M. JAVADI, J. N. JIANG, Electricity and Energy Reliability and Risk Laboratory, School of Electrical and Computer Engineering, University of Oklahoma, Norman, OK, USA
(✉) e-mail: dee.d.wu@ou.edu

Keywords Carbon dioxide emission, Wind generation, System inertia, Rate of change of frequency

1 Introduction

The world-wide concern about carbon dioxide (CO_2) emission has led to the increasing interest in the generation technologies of renewable energy sources. Decarbonization of power generation is crucial for reducing CO_2 emission [1–3]. It is reported that 41 % of the energy-related CO_2 emission are currently from the fossil-fuel power plants, and the percentage is expected to be 44 % in 2030 [4]. To reduce CO_2 emission, the power industry is gradually changing the generation technologies from fossil fuel to renewable energy sources. Among these generation technologies of renewable energy sources, wind generation grows rapidly. It is predicted that, by 2020, the total worldwide power generated by wind generation would be more than 1,261 GW, which can supply about 12 % of total worldwide electricity demand [5].

Such a projected high penetration of wind generation in power systems can affect the frequency stability. Nowadays, most of wind turbines (e.g. Doubly Fed Induction Generators) employ variable speed constant frequency generation technology to produce electric power from variable wind [6]. Normally, variable speed wind turbines do not contribute to system inertia since the rotor of the variable speed wind turbines is running at a variable asynchronous speed and thus not sensitive to the change of system frequency [7–9]. The displacement of a large number of conventional synchronous generators with variable speed wind turbines reduces system inertia. When the system is subjected to an unexpected disturbance that causes a significant system-wide power imbalance, the reduced system inertia can cause a larger and faster

STATE GRID
STATE GRID ELECTRIC POWER RESEARCH INSTITUTE

ROCOF and frequency nadir, which are two critical variables to set the relays for maintaining frequency stability [10–12].

In the study presented in this paper, the impact of the reduction of system inertia on system frequency is analyzed as the consequence of the integration of wind generation into power systems. Then, we investigate the impact of the distribution of the inertia contributions on system frequency in order to answer questions like, 1) when a number of conventional synchronous generators have to be turned off to accommodate more wind power, how important the distribution of the inertia contributions from the remaining online synchronous generators is? 2) for the same amount of system inertia, do different distributions of inertia contributions have different impacts on ROCOF? The answers to these types of questions are useful to better coordinate a conventional synchronous generator fleet for the variable wind power generation. Also, the answers can contribute to developing methods for planning the power generation expansion towards low-carbon economy [13, 14]. Specifically, the investigation is based on the total fault injected energy, which is the additional energy injected into the power system during the fault period. The total fault injected energy is modeled based on the so-called Hamiltonian formulism. The results of the study are demonstrated and explained with the IEEE 39-bus system.

The rest of the paper is organized as follows: in Sect. 2, we analyze the impact of the reduction of system inertia on system frequency; in Sect. 3, a model of total fault injected energy is developed for our study; in Sect. 4, the impact of the distribution of inertia contributions on system frequency is analyzed; Sect. 5 includes the numerical simulations and results of analyses with the IEEE 39-bus system; and Sect. 6 concludes.

2 Impact of reduction of system inertia on frequency

In this section, the impact of the reduction of system inertia is analyzed as the result of the integration of a significant amount of wind generation into power systems.

2.1 Model of power system dynamics

For a power system with N_g interconnected generators and N_b buses, its dynamics can be described by a set of differential and algebraic equations (DAE). That is,

$$\frac{\mathrm{d}\phi_i}{\mathrm{d}t} = \omega_i - \omega_R, \quad i = 1, 2, \ldots, N_g \tag{1}$$

$$M_i \frac{\mathrm{d}(\omega_i - \omega_R)}{\mathrm{d}t} = P_{mi} - P_i, \quad i = 1, 2, \ldots, N_g \tag{2}$$

$$P_i + P_{Li} = 0, \quad i = N_g + 1, N_g + 2, \ldots, N_g + N_b \tag{3}$$

$$Q_i + Q_{Li} = 0, \quad i = N_g + 1, N_g + 2, \ldots, N_g + N_b \tag{4}$$

$$P_i = \sum_{j=1}^{N_g+N_b} B_{ij} V_i V_j \sin(\phi_i - \phi_j), \quad i = 1, 2, \ldots, N_g + N_b$$

$$Q_i = -\sum_{j=1}^{N_g+N_b} B_{ij} V_i V_j \cos(\phi_i - \phi_j), \quad i = 1, 2, \ldots, N_g + N_b$$

where ϕ_i is the i^{th} element of $(N_g + N_b) \times 1$ vector $\boldsymbol{\phi}$ in which the first N_g elements are the rotor angles of the generators in radians and the remaining elements are the bus voltage angles in radians; V_i is the i^{th} element of $(N_g + N_b) \times 1$ vector $\boldsymbol{V}$ in which the first N_g elements are the magnitudes of the generator internal voltages in per unit and the remaining elements are the magnitudes of the bus voltages in per unit; ω_i is the angular velocity of the i^{th} generator in radians per second; ω_R is the rated angular velocity in radians per second; $M_i = 2H_i/\omega_R$ in which H_i is the inertia constant of the i^{th} generator in seconds; P_{mi} is the mechanical power input of the i^{th} generator in per unit; P_i is the real power input at the i^{th} bus in per unit; Q_i is the reactive power input at the i^{th} bus in per unit; P_{Li} and Q_{Li} are the voltage dependent active and reactive power outputs at the i^{th} load bus in per unit, respectively; B_{ij} is the imaginary part of the negative of the branch admittance between buses i and j in per unit; and B_{ii} is the sum of imaginary parts of all branch admittances connected to bus i in per unit.

2.2 Impact of reduction of system inertia on frequency

The impact of the reduction of system inertia on system frequency is analyzed using ROCOF. The ROCOF is the initial slope of the system frequency with respect to time. The ROCOF is an important variable used for relay setting of protection system. Also, the ROCOF is an indicator to measure the seriousness that a disturbance affects system frequency. The ROCOF can be derived from the center of inertia of the system, which has angular velocity below [15],

$$\bar{\omega} = \frac{\sum_{i=1}^{N_g} M_i \omega_i}{\sum_{i=1}^{N_g} M_i} \tag{5}$$

With (5), the ROCOF can be represented as

$$\frac{\mathrm{d}\bar{f}}{\mathrm{d}t} = \frac{-f_R \Delta P_F(0^+)}{\sum_{i=1}^{N_g} 2H_i} \tag{6}$$

where $\mathrm{d}\bar{f}/\mathrm{d}t$ is the ROCOF in hertz per second; f_R is rated system frequency and is selected as 60 Hz; and $\Delta P_F(0^+)$ is

the change in real power output at fault bus F from $t = 0$ to $t = 0^+$ in per unit. The derivation of (6) is presented in Appendix 1.

Equation (6) indicates that system inertia (i.e., the sum of the inertia constants of all generators) can affect the ROCOF. For a fault with a given size, the magnitude of the ROCOF is inversely proportional to system inertia. That is, the lower system inertia is, the larger the magnitude of the ROCOF is. The larger the magnitude of the ROCOF means the more severe frequency drop; thus, the lower system inertia can cause the more severe frequency drop, which may result in frequency instability.

The analysis above shows that frequency stability is a concern in a power system with a large penetration of variable speed wind turbines. Normally, the variable speed wind turbines do not contribute to system inertia. When a large penetration of variable speed wind turbines into a power system reduces the power supplied by conventional synchronous generators, system inertia correspondingly reduces. According to (6), it is known that the reduced system inertia can cause frequency instability when the system is subjected to a significant power imbalance. On the other hand, (6) does not show how the distribution of the inertia contributions from the remaining online synchronous generators affects the ROCOF. The distribution of the inertia contributions may further increase the magnitude of the ROCOF and thus the seriousness of frequency instability. To understand the impact of the distribution of the inertia contributions on system frequency, the ROCOF defined in (6) will be represented based on the total energy injected into the system during the fault period in Sect. 4. A model of the total fault injected energy will be developed in next section.

3 Modeling of total fault injected energy

In this section, a model of total fault injected energy is developed based on Hamiltonian formulism and a classic model of conservative power system.

3.1 Representations of energy components

Let t_c be the fault clearing time and t_s be the time at which the system following a fault is stabilized. The total kinetic and potential energies of the dynamic power system described in (1)–(4) during the period of interest $t \in [t_c, t_s]$ can be summarized as follows:

Total kinetic energy (W_{KE}) can be expressed as,

$$W_{KE} = \frac{1}{2}\sum_{i=1}^{N_g} M_i[\omega_i(t) - \omega_R]^2 \tag{7}$$

Note that the kinetic energy above is represented with the angular velocity relative to the rated angular velocity. More detailed discussion of the total kinetic energy can be found in many references such as [16].

For total potential energy (W_{PE}), which is the electromagnetic energy stored in various components of the power grid, including generators ($W_{PE,1}$), loads ($W_{PE,2}$), and branches ($W_{PE,3}$) in the transmission network, which can be written as,

$$W_{PE} = W_{PE,1} + W_{PE,2} + W_{PE,3} \tag{8}$$

The detailed derivation of (8) can be found in Appendix 2.

According to electric circuit theory [17], these types of potential energy can be further expressed as follows:

1) Potential energy of generators ($W_{PE,1}$) is related to the change in the rotor angle positions of generators, which can be represented as,

$$W_{PE,1} = -\sum_{i=1}^{N_g} P_{mi}(\phi_i(t) - \phi_i(t_s))$$

2) Potential energy of loads ($W_{PE,2}$) includes the potential energy related to both active power ($W_{PE,21}$) and reactive power ($W_{PE,22}$), which can be further written as,

$$\begin{aligned} W_{PE,2} &= W_{PE,21} + W_{PE,22} \\ &= \sum_{i=N_g+1}^{N_g+N_b} \int_{t_s}^{t} P_{Li} \frac{\mathrm{d}\phi_i(\tau)}{\mathrm{d}\tau}\mathrm{d}\tau + \sum_{i=N_g+1}^{N_g+N_b} \int_{V_i(t_s)}^{V_i(t)} \frac{Q_{Li}}{x_i}\mathrm{d}x_i \end{aligned}$$

3) Potential energy stored in branches ($W_{PE,3}$) can be represented as,

$$\begin{aligned} W_{PE,3} = &-\frac{1}{2}\sum_{i=1}^{N_g+N_b}\sum_{j=1}^{N_g+N_b} B_{ij}V_i(t)V_j(t)\cos\big(\phi_i(t) - \phi_j(t)\big) \\ &+\frac{1}{2}\sum_{i=1}^{N_g+N_b}\sum_{j=1}^{N_g+N_b} B_{ij}V_i(t_s)V_j(t_s)\cos\big(\phi_i(t_s) - \phi_j(t_s)\big) \end{aligned}$$

When the offset between the potential energy of loads and branches is considered, the total potential energy can further be described by the potential energy of generators and of branches connected to internal generator buses. Thus, we can have,

$$\begin{aligned} W_{PE} = &-\sum_{i=1}^{N_g} P_{mi}(\phi_i(t) - \phi_i(t_s)) \\ &+\sum_{i=1}^{N_g}\int_{t_s}^{t}\left(\sum_{j=1}^{N_g+N_b} B_{ij}V_i(\tau)V_j(\tau)\sin(\phi_i(\tau) - \phi_j(\tau))\right) \\ &\times\frac{\mathrm{d}\phi_i(\tau)}{\mathrm{d}\tau}\mathrm{d}\tau = \sum_{i=1}^{N_g}\int_{t_s}^{t}(P_i - P_{mi})\frac{\mathrm{d}\phi_i(\tau)}{\mathrm{d}\tau}\mathrm{d}\tau \end{aligned} \tag{9}$$

The detailed derivation of (9) can be found in Appendix 3.

In order to better represent the amount of energy injected into the system during the fault period, which is manifested in the form of kinetic energy, we further separate the integral of (9) into two periods, $[t_s, t_c]$ and $[t_c, t]$. That is, (9) can be rewritten as,

$$W_{PE} = \sum_{i=1}^{N_g} \int_{t_s}^{t_c} (P_i - P_{mi}) \frac{\mathrm{d}\phi_i(\tau)}{\mathrm{d}\tau} \mathrm{d}\tau + \sum_{i=1}^{N_g} \int_{t_c}^{t} (P_i - P_{mi}) \frac{\mathrm{d}\phi_i(\tau)}{\mathrm{d}\tau} \mathrm{d}\tau \tag{10}$$

In (10), it can be seen that the first integral over $[t_s, t_c]$ is a time invariant function with respect to time t while the second integral is a time varying function with respect to time t. The former is considered as an energy constant and selected as a reference. Then, the total potential energy (W_{PE}) of interest can be further simplified as,

$$W_{PE} = \sum_{i=1}^{N_g} \int_{t_c}^{t} (P_i - P_{mi}) \frac{\mathrm{d}\phi_i(\tau)}{\mathrm{d}\tau} \mathrm{d}\tau \tag{11}$$

3.2 Total energy of dynamic power system (Hamiltonian)

The total energy of the power system described in (1)–(4) or Hamiltonian, T, can be constructed based on the total kinetic energy and potential energy described in (7) and (11), respectively. That is,

$$T = W_{KE} + W_{PE} = \frac{1}{2} \sum_{i=1}^{N_g} M_i [\omega_i(t) - \omega_R]^2 + \sum_{i=1}^{N_g} \int_{t_c}^{t} (P_i - P_{mi}) \frac{\mathrm{d}\phi_i(\tau)}{\mathrm{d}\tau} \mathrm{d}\tau \tag{12}$$

The Hamiltonian described in (12) has some features similar to those of the general Hamiltonian in classical mechanics, which is summarized in [18]. The general Hamiltonian is a function with respect to n generalized position coordinates and n generalized momentum coordinates, and the motion characteristics of a dynamic system without dissipation can be described by a set of Hamilton's equations,

$$\frac{\mathrm{d}q_i}{\mathrm{d}t} = \frac{\partial T}{\partial p_i}(q_1, q_2 \ldots, q_n, p_1, p_2 \ldots p_n), \quad i = 1, 2, \ldots, n \tag{13}$$

$$\frac{\mathrm{d}p_i}{\mathrm{d}t} = -\frac{\partial T}{\partial q_i}(q_1, q_2 \ldots, q_n, p_1, p_2 \ldots, p_n), \quad i = 1, 2, \ldots, n \tag{14}$$

where q_i is the i^{th} generalized position coordinate and p_i is the i^{th} generalized momentum coordinate. For a dynamic system consisting of n rigid bodies with mass m_i, $p_i = m_i \dot{q}_i$, $i = 1,2,\ldots,n$.

Let $q_i = \delta_i$ and $p_i = M_i(\omega_i - \omega_R)$. The Hamiltonian in (12) can be viewed as a function with respect to position coordinates and momentum coordinates; with (13)–(14), the Hamilton's equations of the power system described by DAEs in (1)–(4) can be expressed as,

$$\frac{\mathrm{d}\phi_i}{\mathrm{d}t} = \frac{1}{M_i} \frac{\partial (W_{KE} + W_{PE})}{\partial (\omega_i - \omega_R)} = \omega_i - \omega_R, \quad i = 1, 2, \ldots, N_g \tag{15}$$

$$M_i \frac{\mathrm{d}(\omega_i - \omega_R)}{\mathrm{d}t} = -\frac{\partial (W_{KE} + W_{PE})}{\partial \phi_i} = P_{mi} - P_i, \quad i = 1, 2, \ldots, N_g \tag{16}$$

Thus, the derivative of Hamiltonian in (12) with respect to time t can be written as,

$$\begin{aligned} \frac{\mathrm{d}T}{\mathrm{d}t} &= \sum_{i=1}^{N_g} \left(\frac{\partial T}{\partial q_i} \frac{\mathrm{d}q_i}{\mathrm{d}t} + \frac{\partial T}{\partial p_i} \frac{\mathrm{d}p_i}{\mathrm{d}t} \right) \\ &= \sum_{i=1}^{N_g} \left(\frac{\partial (W_{KE} + W_{PE})}{\partial \phi_i} \frac{\mathrm{d}\phi_i}{\mathrm{d}t} + \frac{\partial (W_{KE} + W_{PE})}{\partial (\omega_i - \omega_R)} \frac{\mathrm{d}(\omega_i - \omega_R)}{\mathrm{d}t} \right) \\ &= 0 \end{aligned} \tag{17}$$

Equation (17) confirms that the total system energy during the period $t \in [t_c, t_s]$ is conserved in the power system described by (1)–(4) since the Hamiltonian defined in (12) is a constant during the period. Such confirmation indicates that (12) is a complete expression of the total system energy.

The Hamiltonian during the period $t \in [t_c, t_s]$ is equal to the amount of fault-related energy that is injected into the system at $t = t_c$. Thus, the Hamiltonian during the period $t \in [t_c, t_s]$ can be represented with the total kinetic and potential energies at $t = t_c$ which are described in (7) and (11), respectively,

$$T(t) = T(t_c) = W_{KE}(t_c) + W_{PE}(t_c) = \frac{1}{2} \sum_{i=1}^{N_g} M_i [\omega_i(t_c) - \omega_R]^2 + \sum_{i=1}^{N_g} \int_{t_c}^{t_c} (P_i - P_{mi}) \frac{\mathrm{d}\phi_i(\tau)}{\mathrm{d}\tau} \mathrm{d}\tau = W_{KE}(t_c) \tag{18}$$

Equation (18) is a general representation of the total energy that is injected into the power system during the fault period.

3.3 Numerical estimation of Hamiltonian

The Hamiltonian at $t = t_c$ can be calculated with (18) if the angular velocity of each generator at $t = t_c$ is obtained. Let us consider a small fault with short duration during which the acceleration power for a generator can be

considered a constant. Then, (19) can be obtained from the previous dynamical Eqs. (1)–(4),

$$\omega_i(t_c) - \omega_R \approx -\frac{E_i V_f B_{iF} \cos(\delta_i(0) - \theta_F(0)) \Delta P_F(0^+)}{\sum_{i=1}^{N_g} E_i V_F B_{iF} \cos(\theta_F(0) - \delta_i(0))} \frac{1}{M_i} t_c \tag{19}$$

where E_i is the internal voltage magnitude of the i^{th} generator in per unit; V_F is the pre-fault voltage magnitude at fault bus F in per unit; B_{iF} is the imaginary part of the negative of the transfer admittance between generator internal bus i and fault bus F in per unit; $\delta_i(0)$ is the pre-fault rotor angle of the i^{th} generator at $t = 0$ in radians; and $\theta_F(0)$ is the pre-fault voltage angle of fault bus F in radians. The derivation of (19) is presented in Appendix 4.

Plugging (19) into (18), we have

$$\bar{T}_F(t_c) = \frac{t_c^2}{2} \cdot [\Delta P_F(0^+)]^2 \cdot \sum_{i=1}^{N_g} \frac{1}{M_i} \left[\frac{E_i V_F B_{if} \cos(\delta_i(0) - \theta_F(0))}{\sum_{i=1}^{N_g} E_i V_f B_{iF} \cos(\theta_F(0) - \delta_i(0))} \right]^2 \quad F = 1, 2, \ldots, N_b \tag{20}$$

where $\bar{T}_F(t_c)$ is the estimated Hamiltonian of the system at $t = t_c$ in per unit when a fault occurs at bus F.

Equation (20) indicates that the Hamiltonian is related to three fault factors—fault size, clearing time, and location. The relationship between the Hamiltonian and these three fault factors can be clearly shown by simplifying (20) with assuming $E_i \approx V_F \approx 1$ p.u. and $\cos(\delta_i(0) - \theta_f(0)) \approx 1$,

$$\bar{T}_F(t_c) = \frac{1}{2} \cdot t_c^2 \cdot [\Delta P_F(0^+)]^2 \cdot \sum_{i=1}^{N_g} \frac{B_{iF}^2}{M_i \left[\sum_{i=1}^{N_g} B_{iF} \right]^2}, \quad F = 1, 2, \ldots, N_b \tag{21}$$

Replacing M_i with $H_i/\pi f_R$, (21) becomes

$$\bar{T}_F(t_c) = \frac{\pi f_R}{2} \cdot t_c^2 \cdot [\Delta P_F(0^+)]^2 \cdot \sum_{i=1}^{N_g} \frac{B_{iF}^2}{H_i \left[\sum_{i=1}^{N_g} B_{iF} \right]^2}, \quad F = 1, 2, \ldots, N_b \tag{22}$$

4 Impact of distribution of inertia contributions on frequency

As the result of the integration of a significant amount of wind generation into power systems, the impact of the distribution of inertia contributions from online conventional synchronous generators on system frequency can be analyzed based on the total fault injected energy defined in (22) and the ROCOF defined in (6).

By rewriting (6) based on (22), the impact of the distribution of inertia contributions on the ROCOF can be shown by the following equation:

$$\frac{d\bar{f}}{dt} = -\frac{1}{\sum_{i=1}^{N_g} H_i} \left[\frac{\bar{T}_F(t_c) f_R}{2\pi t_c^2 D_F} \right]^{\frac{1}{2}} \tag{23}$$

where

$$D_F = \sum_{i=1}^{N_g} \frac{B_{iF}^2}{H_i \left[\sum_{i=1}^{N_g} B_{iF} \right]^2}, \quad F = 1, 2, \ldots, N_b \tag{24}$$

Equations (23) and (24) indicate that the distribution of inertia contributions can affect the ROCOF by factor D_F. Equation (23) shows that, for a fault with a given injected energy and clearing time, when system inertia is constant, the magnitude of the ROCOF is inversely proportional to factor D_F. Equation (24) further shows that, for a given fault location, factor D_F depends on the reciprocal of the inertia of each generator, which is related to the distribution of inertia contributions. Thus, for a constant system inertia and a fault with a given injected energy, clearing time and location, when the characteristic of the distribution of inertia contributions increases factor D_f, the magnitude of the ROCOF reduces; when the characteristic of the distribution of inertia contributions reduces factor D_f, the magnitude of the ROCOF increases.

5 Case studies

In this Section, the impact of the distribution of inertia contributions on system frequency is further discussed with example of IEEE 39-bus system shown in Fig. 1. In the system, there are 34 lines, 12 transformers, 39 buses, 10 generators, and 17 loads [19]. Table 1 presents the inertia constant of each generator. In the system, the following two cases are investigated: in Case A, the impact is analyzed in the system under a fault at a given location; in Case B, the impact is analyzed in the system under the fault at different fault locations. In the investigation, the system frequency response is evaluated based on dynamic simulations.

5.1 Impact of distribution of inertia contributions on frequency

At a given fault location, the impact of the distribution of the inertia contributions on frequency response is

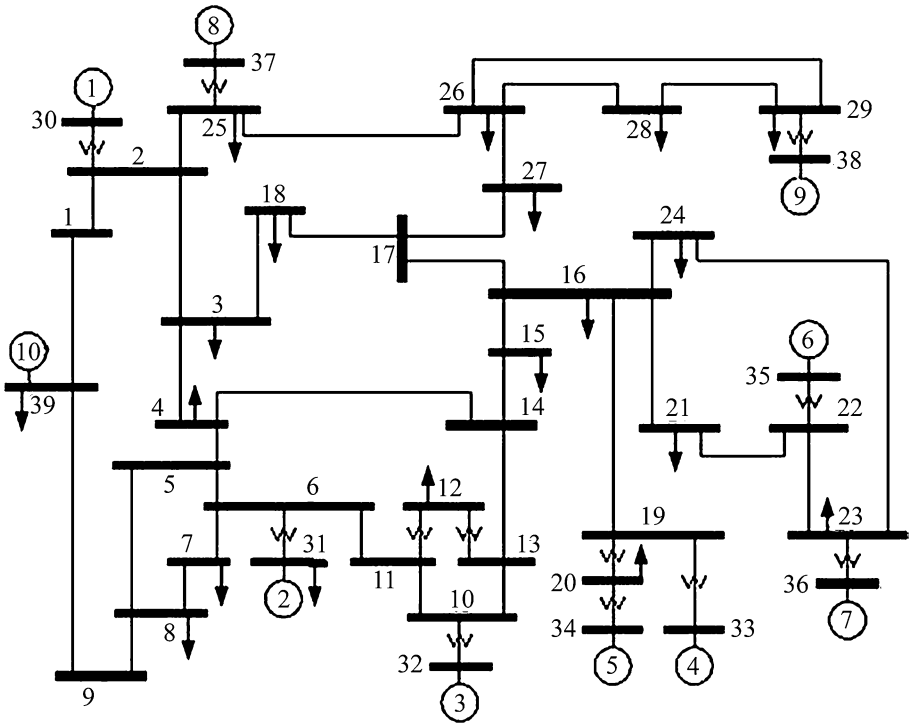

Fig. 1 One-line diagram of the IEEE 39-bus system

Table 1 Generator inertia constants in the IEEE 39-bus system in seconds

H_1	H_2	H_3	H_4	H_5	H_6	H_7	H_8	H_9	H_{10}
42.00	30.50	35.80	28.60	26.00	34.80	26.40	24.30	34.50	500.00

investigated using different scenarios of the inertia constants, which are shown in Table 2. In each scenario, system inertia is the same, but the dispersion of the distribution of the inertia constants is different. The dispersion is quantified by calculating the standard deviation of all inertia constants. For a given scenario, the three-phase fault with a given injected energy is applied in bus 39 at $t = 0$ s and then is cleared at $t_c = 0.15$ s in the system. Figure 2 shows the change of the ROCOF with the dispersion of the distribution of the inertia contributions. Figure 3 shows the change of factor D_F in (23) with the dispersion of the distribution of the inertia contributions.

It is observed from Fig. 2 that the distribution of the inertia contributions significantly affects the magnitude of the ROCOF. In Fig. 2, the magnitude of the ROCOF increases with the dispersion of the distribution of the inertia contributions when the system is subjected to a fault with a given injected energy, location, and clearing time. This indicates that the seriousness of the impact of the fault at bus 39 on the system frequency response increases with the dispersion of the distribution of the inertia contributions.

Figure 3 shows that the observation from Fig. 2 is consistent with the analysis results of (23) and (24). According to (23), it is known that the magnitude of the ROCOF increases with the decrease in factor D_F when the system with a constant system inertia is subjected to a fault with a given injected energy, location, and clearing time. Equation (24) shows that the distribution of inertia contributions can change factor D_F. In Fig. 3, factor D_F reduces when the dispersion of the distribution of the inertia contributions increases. According to (23), the magnitude of the ROCOF increases with the dispersion of the distribution of the inertia contributions. This is consistent with the observation from Fig. 2.

5.2 Impact of distribution of inertia contributions and fault locations on frequency

At different fault locations, the impact of the distribution of inertia contributions on frequency response is investigated using the same scenarios of the inertia constants shown in Table 2. For a given scenario, the three-phase fault that is used in Sect. 5.1 is separately applied to buses 30, 33, 35, and 36. Figures 4, 5 show the changes of the ROCOF and factor D_F with the dispersion of the distribution of the inertia contributions in the system under the fault at different locations, respectively. Figure 6 shows the

Table 2 Different scenarios of generator inertia constants in the IEEE 39-bus system in seconds

	S_1	S_2	S_3	S_4	S_5	S_6	S_7	S_8	S_9	S_{10}	S_{11}
H_1	88.67	84.00	79.33	74.67	70.00	65.33	60.67	56.00	51.33	46.67	42.00
H_2	76.97	72.30	67.63	62.97	58.30	53.63	48.97	44.30	39.63	34.97	30.30
H_3	82.47	77.80	73.13	68.47	63.80	59.13	54.47	49.80	45.13	40.47	35.80
H_4	75.27	70.60	65.93	61.27	56.60	51.93	47.27	42.60	37.93	33.27	28.60
H_5	72.67	68.00	63.33	58.67	54.00	49.33	44.67	40.00	35.33	30.67	26.00
H_6	81.47	76.80	72.13	67.47	62.80	58.13	53.47	48.80	44.13	39.47	34.80
H_7	73.07	68.40	63.73	59.07	54.40	49.73	45.07	40.40	35.73	31.07	26.40
H_8	70.97	66.30	61.63	56.97	52.30	47.63	42.97	38.30	33.63	28.97	24.30
H_9	81.17	76.50	71.83	67.17	62.50	57.83	53.17	48.50	43.83	39.17	34.50
H_{10}	80.00	122.00	164.00	206.00	248.00	290.00	332.00	374.00	416.00	458.00	500.00
Sum	782.70	782.70	782.70	782.70	782.70	782.70	782.70	782.70	782.70	782.70	782.70
Standard deviation	5.19	15.46	29.04	42.89	56.81	70.77	84.73	98.71	112.69	126.68	140.67

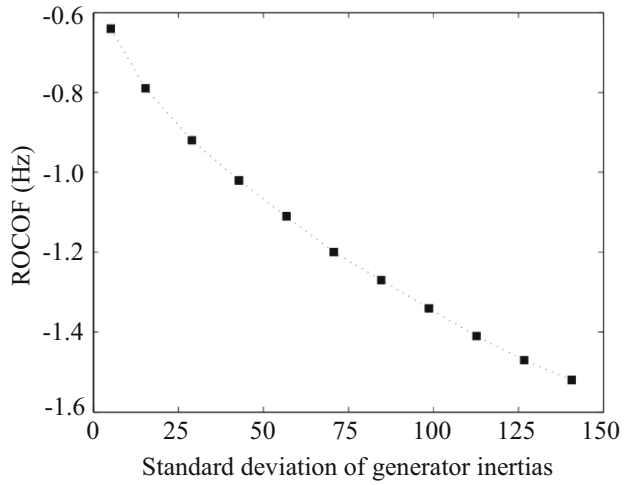

Fig. 2 Change of the ROCOF with the dispersion of the distribution of the inertia contributions in the IEEE 39-bus system under the fault at bus 39

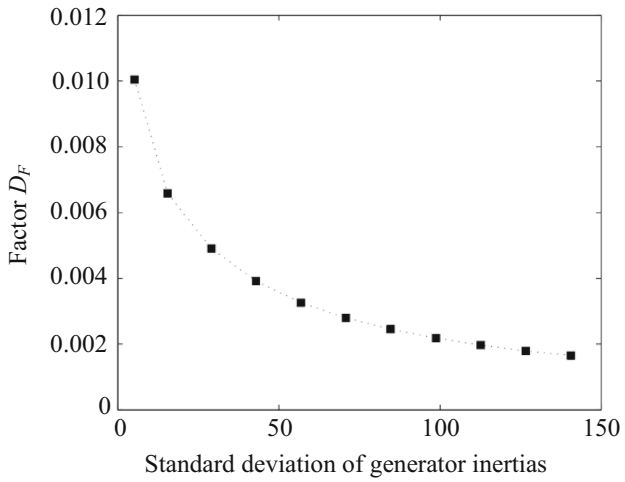

Fig. 3 Change of factor D_F with the dispersion of the distribution of the inertia contributions in the IEEE 39-bus system under the fault at bus 39

comparison of the ROCOFs at different fault locations in different scenarios of the inertia constants.

Figures 4, 5 show that the changes of the ROCOF with the dispersion of the distribution of the inertia contributions in the system under the fault at different locations are consistent with the analysis results of (23) and (24). According to (23) and (24), it is known that the magnitude of the ROCOF reduces with the increase in factor D_F when the system with a constant system inertia is subjected to a fault with a given injected energy, location, and clearing time. In Fig. 5, when the system is subjected to the fault at buses 30, 33, 35, or 36, factor D_F increases with the dispersion of the distribution of the inertia contributions. Thus, when the system is subjected to the fault at these buses, the magnitude of the ROCOF reduces with the increase in the dispersion of the distribution of the inertia contributions. This is consistent with the results shown in Fig. 4.

More importantly, Fig. 6 and Table 2 show that the average of the magnitudes of the ROCOF caused by the fault at different fault locations increases with the dispersion of the distribution of the inertia contributions. It can be seen from Fig. 6 and Table 2 that when the fault occurs at bus 30, 33, 35, or 36, the magnitude of the ROCOF reduces with the increase in the dispersion of the distribution of the inertia contributions; however, when the fault occurs at bus 39, the magnitude of the ROCOF increases with the dispersion of the distribution of the inertia contributions. Also, Fig. 6 shows that, in most of scenarios of inertia constants, the magnitude of the ROCOF caused by the fault at bus 39 is much larger than that caused by the fault at bus 30, 33, 35, or 36. Thus, the average of the magnitudes of the ROCOF caused by the fault at these buses increases with the dispersion of the distribution of the inertia contributions.

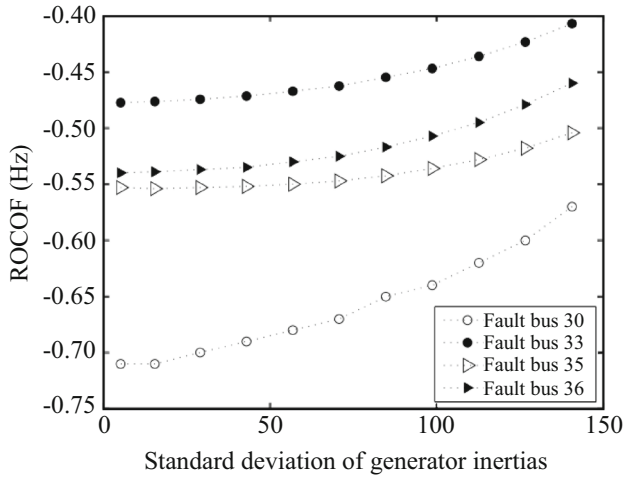

Fig. 4 Changes of the ROCOF with the dispersion of the distribution of the inertia contributions in the IEEE 39-bus system under the fault at different locations

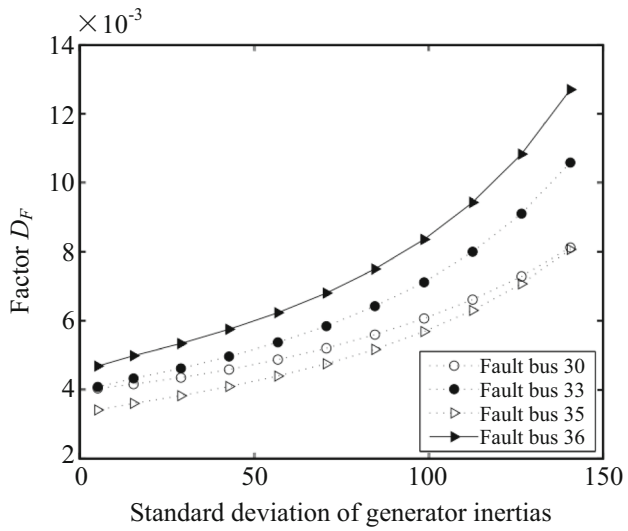

Fig. 5 Changes of factor D_F with the dispersion of the distribution of the inertia contributions in the IEEE 39-bus system under the fault at different fault locations

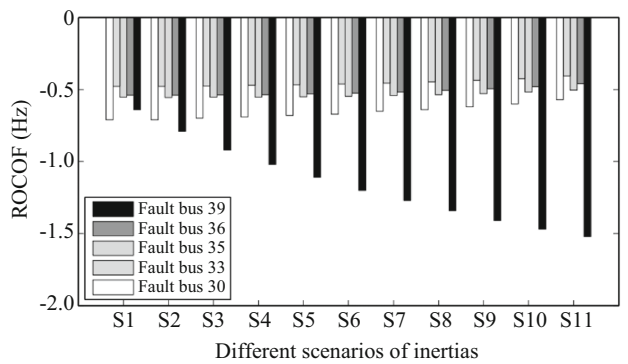

Fig. 6 Comparison of the ROCOFs at different fault locations in different scenarios of the inertia constants

6 Conclusions

This paper discussed the impact of the reduction of system inertia on system frequency as the result of the high penetration of wind generation into power systems. Moreover, a preliminary study of the impact of the distribution of inertia contributions on system frequency was included. In the study, the impact of the distribution of inertia contributions on the ROCOF was investigated based on the total energy injected to the power system during the fault period. The total fault energy was represented using Hamiltonian formulism. With the IEEE 39-bus system, it was shown that, for a fault with a given injected energy, clearing time, and location, the distribution of the inertia contributions can significantly affect the magnitude of the ROCOF; furthermore, for a given (sized) fault at different locations, the average of the magnitudes of the ROCOF caused by the fault is larger when the distribution of the inertia contributions is more dispersed.

The implications of the study presented in this paper to the development of the low-carbon electric power system are: 1) if the concern about frequency stability resulting from the reduction of system inertia and the distribution of inertia contributions are indeed a serious concern in the development of the low-carbon power system, the online synchronous generator fleet needs a better coordination to accommodate the variable wind power; 2) frequency stability should be seriously studied for the development of the low-carbon electric power system with the high penetration of renewable energy sources, especially for those associated with the initial frequency response in the system following a power imbalance.

Appendix 1

Derivation of (6)

Based on (5), the mean acceleration of all generators in the system at $t = 0^+$ can be represented as,

$$\frac{\mathrm{d}\bar{\omega}(0^+)}{\mathrm{d}t} = \frac{\sum_{i=1}^{N_g} M_i \frac{\mathrm{d}\omega_i(0^+)}{\mathrm{d}t}}{\sum_{i=1}^{N_g} M_i} \tag{25}$$

In (25), the acceleration of the i^{th} generator at $t = 0^+$ can be expressed as,

$$\frac{\mathrm{d}\omega_i(0^+)}{\mathrm{d}t} = \frac{-\Delta P_{ei}(0^+)}{M_i} \tag{26}$$

where $\Delta P_{ei}(0^+)$ is the change in the real power output of the i^{th} generator from $t = 0$ to $t = 0^+$ in per unit and can be represented with (27) below by using a typical treatment of a small fault.

$$\Delta P_{ei}(0^+) = -E_i V_F B_{iF} \cos(\delta_i(0) - \theta_F(0))\Delta\theta_F \tag{27}$$

where $\theta_F(0)$ can be further represented as,

$$\Delta\theta_F = \frac{-\Delta P_F(0^+)}{\sum_{i=1}^{N_g} V_i V_f B_{iF} \cos(\theta_F(0) - \delta_i(0))} \tag{28}$$

With (26)–(28), (25) can be rewritten as,

$$\frac{\mathrm{d}\bar{\omega}(0^+)}{\mathrm{d}t} = -\frac{\Delta P_F(0^+)}{\sum_{i=1}^{N_g} M_i} \tag{29}$$

Replacing $\bar{\omega}(0^+)$ and M_i with $2\pi\bar{f}$ and $H_i/\pi f_{\mathrm{R}}$, respectively, (29) becomes

$$\frac{\mathrm{d}\bar{f}}{\mathrm{d}t} = -\frac{f_R \Delta P_F(0^+)}{\sum_{i=1}^{N_g} 2H_i} \tag{30}$$

Appendix 2

Derivation of (8)

In (8), the components of potential energy are defined according to (31) below, which is derived from (1)–(4).

$$\begin{aligned}
&\sum_{i=1}^{N_g} \frac{1}{2} M_i[\omega_i(t) - \omega_R]^2 = \sum_{i=1}^{N_g} P_{mi}[\phi_i(t) - \phi_i(t_s)] \\
&\quad - \int_{t_s}^{t} \sum_{i=N_g+1}^{N_g+N_b} P_{Li}(V_i) \frac{\mathrm{d}\phi_i(\tau)}{\mathrm{d}\tau}\mathrm{d}\tau - \int_{t_s}^{t} \sum_{i=N_g+1}^{N_g+N_b} \frac{Q_{Li}}{V_i}\frac{\mathrm{d}V_i}{\mathrm{d}\tau}\mathrm{d}\tau \\
&\quad + \frac{1}{2}\sum_{i=1}^{N_g+N_b}\sum_{j=1}^{N_g+N_b} \left[B_{ij} V_i(t) V_j(t) \cos(\phi_i(t) - \phi_j(t))\right] \\
&\quad - \frac{1}{2}\sum_{i=1}^{N_g+N_b}\sum_{j=1}^{N_g+N_b} \left[B_{ij} V_i(t_s) V_j(t_s) \cos(\phi_i(t_s) - \phi_j(t_s))\right] \\
&= -W_{PE,1} - \left(W_{PE,21} + W_{PE,22}\right) - W_{PE,3} \\
&= -\left(W_{PE,1} + W_{PE,2} + W_{PE,3}\right)
\end{aligned} \tag{31}$$

Equation (31) is derived as follows:

1) Both sides of (2) are multiplied by $(\mathrm{d}\phi_i/\mathrm{d}t)$ and then the summation of N_g generator equations yields

$$\sum_{i=1}^{N_g} M_i(\omega_i - \omega_R)\frac{\mathrm{d}(\omega_i - \omega_R)}{\mathrm{d}t} = \sum_{i=1}^{N_g}(P_{mi} - P_i)\frac{\mathrm{d}\phi_i}{\mathrm{d}t} \tag{32}$$

When $\omega_i(t_s) = \omega_R$, the integral of both sides of (32) from t to t_s can be represented as,

$$\begin{aligned}
&\sum_{i=1}^{N_g} \frac{1}{2} M_i[\omega_i(t) - \omega_R]^2 = -W_{PE,1} \\
&\quad - \int_{t_s}^{t} \sum_{i=1}^{N_g}\sum_{j=1}^{N_g+N_b} B_{ij} V_i V_j \sin(\phi_i - \phi_j)\frac{\mathrm{d}\phi_i}{\mathrm{d}\tau}\mathrm{d}\tau = 0
\end{aligned} \tag{33}$$

2) Both sides of (3) are multiplied by $(\mathrm{d}\phi_i/\mathrm{d}t)$, and then the summation of N_b equations yields the following equation,

$$\sum_{i=N_g+1}^{N_g+N_b} P_i \frac{\mathrm{d}\phi_i}{\mathrm{d}t} + \sum_{i=N_g+1}^{N_g+N_b} P_{Li}\frac{\mathrm{d}\phi_i}{\mathrm{d}t} = 0 \tag{34}$$

The integral of both sides of (34) from t to t_s can be represented as follows,

$$\begin{aligned}
&-\int_{t_s}^{t} \sum_{i=N_g+1}^{N_g+N_b}\sum_{j=1}^{N_g+N_b} B_{ij} V_i V_j \sin(\phi_i - \phi_j)\frac{\mathrm{d}\phi_i}{\mathrm{d}\tau}\mathrm{d}\tau \\
&\quad - \int_{t_s}^{t} \sum_{i=N_g+1}^{N_g+N_b} P_{Li}\frac{\mathrm{d}\phi_i}{\mathrm{d}\tau}\mathrm{d}\tau \\
&= -\int_{t_s}^{t} \sum_{i=N_g+1}^{N_g+N_b}\sum_{j=1}^{N_g+N_b} B_{ij} V_i V_j \sin(\phi_i - \phi_j)\frac{\mathrm{d}\phi_i}{\mathrm{d}\tau}\mathrm{d}\tau \\
&\quad - W_{PE,21} = 0
\end{aligned} \tag{35}$$

3) Both sides of (4) are divided by V_i and then multiplied by $(\mathrm{d}V_i/\mathrm{d}t)$; the summation of N_b equations yields the equation below,

$$\sum_{i=N_g+1}^{N_g+N_b} \frac{Q_{Li}}{V_i}\frac{\mathrm{d}V_i}{\mathrm{d}t} + \sum_{i=N_g+1}^{N_g+N_b} \frac{Q_i}{V_i}\frac{\mathrm{d}V_i}{\mathrm{d}t} = 0 \tag{36}$$

Since $\mathrm{d}E_i/\mathrm{d}t = 0$ at the internal generator bus, the left-hand-side second term of (36) can be represented with the summation of $N_g + N_b$ equations; then (36) can be changed as,

$$\sum_{i=N_g+1}^{N_g+N_b} \frac{Q_{Li}}{V_i}\frac{\mathrm{d}V_i}{\mathrm{d}t} + \sum_{i=1}^{N_g+N_b} \frac{Q_i}{V_i}\frac{\mathrm{d}V_i}{\mathrm{d}t} = 0 \tag{37}$$

The integral of both sides of (37) from t to t_s can be represented with the equation below

$$\begin{aligned}
&-\int_{t_s}^{t} \sum_{i=N_g+1}^{N_g+N_b} \frac{Q_{Li}}{V_i(\tau)}\frac{\mathrm{d}V_i(\tau)}{\mathrm{d}\tau}\mathrm{d}\tau + \int_{t_s}^{t} \sum_{i=1}^{N_g+N_b}\sum_{j=1}^{N_g+N_b} \\
&\quad \times B_{ij} V_j(\tau)\cos\left(\phi_i(\tau) - \phi_j(\tau)\right)\frac{\mathrm{d}V_i(\tau)}{\mathrm{d}\tau}\mathrm{d}\tau = -W_{PE,22} \\
&\quad + \int_{t_s}^{t} \sum_{i=1}^{N_g+N_b}\sum_{j=1}^{N_g+N_b} B_{ij} V_j(\tau)\cos\left(\phi_i(\tau) - \phi_j(\tau)\right)\frac{\mathrm{d}V_i(\tau)}{\mathrm{d}\tau}\mathrm{d}\tau = 0
\end{aligned} \tag{38}$$

4) Eq. (31) can be obtained by summating (33), (35), and (38). Note that in addition to the total kinetic energy and negative potential energy components $W_{PE,1}$, $W_{PE,21}$, $W_{PE,22}$, the remanding terms in these equations can be integrated and then represented with negative potential energy component $W_{PE,3}$. The details can be found in Appendix 3.

Appendix 3

Derivation of (9)

The potential energy of branches ($W_{PE,3}$) can be reorganized as follows:

$$\begin{aligned} W_{PE,3} = &- \sum_{i=1}^{N_g+N_b} \frac{1}{2} B_{ii} V_i^2(t) + \sum_{i=1}^{N_g+N_b} \frac{1}{2} B_{ii} V_i^2(t_s) \\ &- \sum_{i=1}^{N_g+N_b-1} \sum_{j=i+1}^{N_g+N_b} B_{ij} V_i(t) V_j(t) \cos\big(\phi_i(t) - \phi_j(t)\big) \\ &+ \sum_{i=1}^{N_g+N_b-1} \sum_{j=i+1}^{N_g+N_b} B_{ij} V_i(t_s) V_j(t_s) \cos\big(\phi_i(t_s) - \phi_j(t_s)\big) \end{aligned} \tag{39}$$

Equation (39) can be represented with the integral form below,

$$\begin{aligned} W_{PE,3} = &- \int_{t_s}^{t} \sum_{i=1}^{N_g+N_b} B_{ii} V_i(\tau) \frac{\mathrm{d}V_i(\tau)}{\mathrm{d}\tau} \mathrm{d}\tau \\ &- \int_{t_s}^{t} \sum_{i=1}^{N_g+N_b-1} \sum_{j=i+1}^{N_g+N_b} B_{ij} \cos\big(\phi_i(\tau) - \phi_j(\tau)\big) \\ &\times \left(V_j(\tau) \frac{\mathrm{d}V_i(\tau)}{\mathrm{d}\tau} + V_i(\tau) \frac{\mathrm{d}V_j(\tau)}{\mathrm{d}\tau} \right) \mathrm{d}\tau \\ &+ \int_{t_s}^{t} \sum_{i=1}^{N_g+N_b-1} \sum_{j=i+1}^{N_g+N_b} B_{ij} V_i(\tau) V_j(\tau) \sin\big(\phi_i(\tau) - \phi_j(\tau)\big) \\ &\frac{\mathrm{d}\big(\phi_i(\tau) - \phi_j(\tau)\big)}{\mathrm{d}\tau} \mathrm{d}\tau \\ = &- \int_{t_s}^{t} \sum_{i=1}^{N_g+N_b} B_{ii} V_i(\tau) \frac{\mathrm{d}V_i(\tau)}{\mathrm{d}\tau} \mathrm{d}\tau \\ &- \int_{t_s}^{t} \sum_{i=1}^{N_g+N_b} \sum_{j=1, j\neq i}^{N_g+N_b} B_{ij} V_j(\tau) \cos\big(\phi_i(\tau) - \phi_j(\tau)\big) \frac{\mathrm{d}V_i(\tau)}{\mathrm{d}\tau} \mathrm{d}\tau \\ &+ \int_{t_s}^{t} \sum_{i=1}^{N_g+N_b} \sum_{j=1}^{N_g+N_b} B_{ij} V_i(\tau) V_j(\tau) \sin\big(\phi_i(\tau) - \phi_j(\tau)\big) \frac{\mathrm{d}\phi_i(\tau)}{\mathrm{d}\tau} \mathrm{d}\tau \end{aligned}$$

With (3) and (4), the equation above can be simplified as,

$$\begin{aligned} W_{PE,3} = &- \int_{t_s}^{t} \sum_{i=N_g+1}^{N_g+N_b} \frac{Q_{Li}}{V_i} \frac{\mathrm{d}V_i}{\mathrm{d}\tau} \mathrm{d}\tau - \int_{t_s}^{t} \sum_{i=N_g+1}^{N_g+N_b} P_{Li} \frac{\mathrm{d}\phi_i(\tau)}{\mathrm{d}\tau} \mathrm{d}\tau \\ &+ \int_{t_s}^{t} \sum_{i=1}^{N_g} \sum_{j=1}^{N_g+N_b} B_{ij} V_i(\tau) V_j(\tau) \sin\big(\phi_i(\tau) \\ &- \phi_j(\tau)\big) \frac{\mathrm{d}\phi_i(\tau)}{\mathrm{d}\tau} \mathrm{d}\tau = -W_{PE,2} + \int_{t_s}^{t} \sum_{i=1}^{N_g} \sum_{j=1}^{N_g+N_b} \\ &\times B_{ij} V_i(\tau) V_j(\tau) \sin\big(\phi_i(\tau) - \phi_j(\tau)\big) \frac{\mathrm{d}\phi_i(\tau)}{\mathrm{d}\tau} \mathrm{d}\tau \end{aligned} \tag{40}$$

Plugging (40) into (8), we have (9). That is,

$$\begin{aligned} W_{PE} = &- \sum_{i=1}^{N_g} P_{mi} \big(\phi_i(t) - \phi_i(t_s)\big) \\ &+ \sum_{i=1}^{N_g} \int_{t_s}^{t} \left(\sum_{j=1}^{N_g+N_b} B_{ij} V_i(\tau) V_j(\tau) \sin\big(\phi_i(\tau) - \phi_j(\tau)\big) \right) \\ &\times \frac{\mathrm{d}\phi_i(\tau)}{\mathrm{d}\tau} \mathrm{d}\tau = \sum_{i=1}^{N_g} \int_{t_s}^{t} (P_i - P_{mi}) \frac{\mathrm{d}\phi_i(\tau)}{\mathrm{d}\tau} \mathrm{d}\tau \end{aligned}$$

Appendix 4

Derivation of (19)

The angular velocity of a generator relative to the rated angular velocity at $t = t_c$ can be represented with the change in angular velocity of the generator from $t = 0$ to $t = t_c$,

$$\omega_i(t_c) - \omega_R = \Delta\omega_i(t_c) = (\omega_i(t_c) - \omega_R) - (\omega_i(0) - \omega_R), \quad i = 1, 2, \ldots, N_g \tag{1}$$

where the angular velocity of a generator is assumed to be equal to the rated angular velocity (i.e., $\omega_i(0) = \omega_R$) before a fault occurs.

The change in the angular velocity of the generator in (41) can be represented with the integral of the acceleration of the generator during the period $t \in (0, t_c)$,

$$\Delta\omega_i(t_c) = \int_{0^+}^{t_c^-} \frac{\mathrm{d}\omega_i(\tau)}{\mathrm{d}\tau} \mathrm{d}\tau, \quad i = 1, 2, \ldots, N_g \tag{42}$$

For a short duration of fault, the acceleration power of a generator can be considered as a constant that is equal to the change in the real power output of the generator from $t = 0$ to $t = 0^+$. Thus, the acceleration of the generator can be considered as a constant during the duration of fault. Then, (42) can be represented as,

$$\Delta\omega_i(t_c) = \int_{0^+}^{t_c^-} \frac{\mathrm{d}\omega_i(\tau)}{\mathrm{d}\tau}\mathrm{d}t = \frac{\mathrm{d}\omega_i(0^+)}{\mathrm{d}t}t_c = -\Delta P_{ei}(0^+)\frac{1}{M_i}t_c, \quad i = 1, 2, \ldots, N_g \tag{43}$$

With (27)–(28) and (43), the angular velocity of a generator relative to the rated angular velocity at $t = t_c$ can be approximately represented as,

$$\omega_i(t_c^-) - \omega_R = -\frac{E_i V_F B_{iF}\cos(\delta_i(0) - \theta_F(0))\Delta P_F(0^+)}{\sum_{i=1}^{N_g} V_i V_F B_{iF}\cos(\theta_F(0) - \delta_i(0))}\frac{1}{M_i}t_c$$

References

[1] Metz B (2005) IPCC special report on carbon dioxide capture and storage. Cambridge University Press, Cambridge

[2] Intergovernmental Panel for Climate Change (2005) Fourth Assessment Report. Cambridge University Press, Cambridge

[3] Committee on Climate Change (2008) Building a low-carbon economy—the UK's contribution to tackling climate change. The Stationary Office, London

[4] Internal Energy Agency (2006) World energy outlook 2006. Renouf Pub Co Ltd, Rochford

[5] European Wind Energy Association (EWEA) (2002) Wind Force 12. EWEA, Brussels

[6] Muller S, Deicke M, De Doncker RW (2002) Doubly fed induction generator systems for wind turbines. IEEE Ind Appl Mag 8(3):26–33

[7] Lalor G, Mullane A, O'Malley M (2005) Frequency control and wind turbine technologies. IEEE Trans Power Syst 20(4):1905–1913

[8] Reza M, Morren J, Schavemaker PH et al (2005) Power electronic interfaced DG units: impact of control strategy on power system transient stability. In: Proceedings of the 3rd IEEE international conference on reliability in transmission and distribution network (RTDN'05), 15–17 Feb 2005, London, pp 179–182

[9] Morren J, Pierik J, De Hann SWH (2006) Inertial response of variable speed wind turbines. Electr Power Syst Res 76(11):980–987

[10] Anderson PM, Mirheydar M (1992) An adaptive method for setting underfrequency load shedding relays. IEEE Trans Power Syst 7(2):647–655

[11] Drukin CJ, Eberle ER, Zarakas P (1969) An underfrequency relay with frequency decay compensation. IEEE Trans Power Appar Syst 88(6):812–820

[12] Farrokhseresht N, Orostica HC, Hesamzadeh MR (2014) Determination of acceptable inertia limit for ensuring adequacy under high levels of wind integration. In: Proceedings of the 11th international conference on the European energy market (EEM'14), 28–30 May 2014, Krakow, 5 pp

[13] Careri F, Genesi C, Marannino P et al (2011) Generation expansion planning in the age of green economy. IEEE Trans Power Syst 26(4):2214–2223

[14] Chen QX, Kang CQ, Xia Q et al (2010) Power generation expansion planning model towards low-carbon economy and its application in China. IEEE Trans Power Syst 25(2):1117–1125

[15] Anderson PM, Fouad AA (2003) Power system control and stability. IEEE Press, Piscataway

[16] Sauer PW, Pai MA (1998) Power system dynamics and stability. Prentice-Hall, Englewood Cliffs

[17] Alexander CK, Sadiku MNO (2007) Fundamentals of electric circuits, 3rd edn. McGraw-Hill, Boston

[18] Greiner W (2010) Classical mechanics: Systems of particles and Hamiltonian dynamics. Springer, Berlin

[19] Pai MA (1989) Energy function analysis for power system stability. Kluwer Academic Publishers, Boston

Di WU is currently the research scientist and instructor at the Electricity and Energy Reliability and Risk Laboratory in the School of Electrical and Computer Engineering at the University of Oklahoma. He received his first Ph.D degree in electrical engineering from Zhejiang University in China, and another Ph.D degree in applied complex networks from Politecnico Di Torino in Italy. His research interests include power grid cascading failure analysis and application of advanced complex networks methods in power systems.

Milad JAVADI is currently working toward his Ph.D. degree in the School of Electrical and Computer Engineering at the University of Oklahoma. His research interests include power system operation, statistical and data analysis in power system, and power economics.

John Ning JIANG is OG&E chair professor in electrical engineering and director of the Electricity and Energy Reliability and Risk Laboratory in the School of Electrical and Computer Engineering at the University of Oklahoma. His current research interest is to understand various types of risks in power system operation and the power market.